Acta Cryst. (1999). A**55**, 119–126

Simulations for imaging with atomic focusers

R. E. Dunin-Borkowski[a] and J. M. Cowley[b]*

[a]*Center for Solid State Science, Arizona State University, Tempe, AZ 85287-1704, USA, and* [b]*Department of Physics and Astronomy, Arizona State University, Tempe, AZ 85287-1504, USA. E-mail: cowley@asm.edu*

(*Received 2 February 1998; accepted 15 May 1998*)

Dedicated to Professor A. F. Moodie on the occasion of his 75th birthday

Abstract

The basis has been explored for the possible application of the various schemes that have been proposed for making use of the focusing properties of single heavy atoms, or rows of atoms extending through thin crystals in axial directions, for the attainment of ultra-high resolution in electron microscopy. Calculations are reported for the form of 200 keV electron beams channeled along rows of atoms through crystals and propagated in the vacuum beyond the crystals. The conditions for forming beams less than 0.05 nm in diameter have been established. Simulations of images having resolutions of this order are reported for the case that the specimen is placed at the Fourier image position beyond the exit face of a thin crystal and the transmission of the periodic array of ultra-fine beams, translated laterally by tilting the incident beam, may be observable using a conventional transmission-electron-microscopy (TEM) instrument.

1. Introduction

It was proposed in an earlier paper (Cowley *et al.*, 1997) that it may be possible to take advantage of the focusing action of the potential field of a single heavy atom, or of a row of atoms extending through a thin crystal (an 'atomic focuser'), to improve the resolution limits for electron microscopy with 100 to 400 keV electrons from the present limits of 0.15 to 0.2 nm to the range of 0.05 nm or better.

An atomic focuser, illuminated by a plane electron wave, or by the probe formed by a scanning transmission-electron-microscopy (STEM) instrument, forms a crossover of diameter less than 0.05 nm at a distance of 1–2 nm beyond the exit face. Such a probe could be used as the basis for a STEM instrument having a resolution of better than 0.05 nm provided that some means can be found for scanning the probe over the specimen. The piezoelectric positioning and scanning mechanism used for scanning probe microscopies may be suitable for this purpose. However, other imaging modes appear possible when it is considered that, according to the reciprocity principle, for any STEM mode there should be an equivalent mode of fixed-beam transmission electron microscopy (TEM). Also, if a thin crystal is used as a periodic multiple array of atomic focusers, the set of fine probes at the exit face of the crystal is reproduced at the Fourier image distances (multiples of $2a^2/\lambda$ for a periodicity a and wavelength λ) (Cowley & Moodie, 1957) so that the distance of the atomic focuser from the specimen may be as large as 100 nm or more and scanning of the probes across the specimen may be accomplished simply by tilting the incident beam. Then no relative motion of the specimen and the focuser is required.

In subsequent papers, some initial computer simulations for several of the suggested imaging modes have been reported. It has been shown that, for a specimen consisting of two Au atoms about 0.05 nm apart, the images should show the atoms with good contrast, clearly resolved. Sanchez & Cowley (1998) showed that, if a column of atoms in a very thin crystal of gold is used as an atomic focuser to form the very short focus objective lens of a TEM system, the image of a region up to 0.28 nm in diameter could be imaged. If each specimen region of such a diameter is illuminated in turn by a narrow incident beam (for example, from a STEM instrument), the whole area of an extended specimen may be imaged with better than 0.05 nm resolution.

Cowley *et al.* (1998) showed that if such a specimen is placed at the first Fourier image plane of a thin Au[001] crystal, 33.2 nm from the specimen, and images are recorded for a series of tilts of the incident beam using a standard TEM, having 0.2 nm resolution, the series of images may be correlated to give a single image of an extended region with 0.05 nm resolution or better.

These simulations suggest that all of the six modes suggested in the original paper of Cowley *et al.* (1997) should be capable of giving ultra-high-resolution images if suitable experimental arrangements can be made. However, many more simulations are required in order to establish the instrumental requirements and the ranges of the experimental variables for optimum imaging. In particular, it is necessary to establish such properties as the field of view and depth of focus for the imaging and the optimum structures and thicknesses for crystals to be used as multiple atomic focusers. In this

ISSN 0108-7673

paper, we report simulations that provide answers to some of the most urgent of these needs. The simulations have been made with multislice algorithms written in the Semper image processing language (Saxton *et al.*, 1979) on a Silicon Graphics workstation.

2. Transmission through atomic focuser crystals

A number of reports have been published of simulations of the electron transmission through crystals in directions of high symmetry (Fertig & Rose, 1981; Marks, 1985; Loane *et al.*, 1988; Broeckx *et al.*, 1995) in connection with the channeling of electrons along columns of atoms and its implications for high-resolution TEM imaging, the contrast of STEM imaging with a high-angle annular detector and the generation of secondary radiations from the atoms. It has been established that there is a characteristic periodicity of the wave field along the atomic columns which is dependent on the atomic numbers of the atoms present.

In Fig. 1, a more detailed description is given of the transmission of 200 keV electrons along the rows of Au atoms in an Au[001] crystal in terms of the amplitude, phase and width of the peaks along the centers of the columns of atoms for the two atom positions of the unit cell, with coordinates (0, 0) and (0.5, 0), which are nonequivalent for dynamical diffraction. The multislice calculations were made with a slice thickness equal to 1/8 of the unit-cell periodicity and atomic scattering factors extrapolated linearly as a function of angle from the tabulated X-ray f values of Rez *et al.* (1994). The amplitude is seen to vary almost sinusoidally with a periodicity of 5.56 nm, with a superimposed small oscillation having the periodicity of the spacing of Au atoms along the columns. The expected 0.2 nm difference in the maxima positions for the two atom positions is visible. The peak widths (full width at half-maximum) have a minimum value of 0.029 nm but are less than 0.041 nm for most thicknesses. For thicknesses that are close to multiples of 5.56 nm, the peaks are not sufficiently well defined to allow a width to be assigned to them because the wavefunction approximates to the plane wave of the incident beam. Apart from the small oscillations with the unit-cell periodicity, the phases increase steadily with thickness, increasing by 2π for each 5.56 nm periodicity.

If the same calculation is made for a plane wave incident with a slice thickness of one unit cell for the multislice calculations, the amplitude, phase and width variations are very close to those of Fig. 1, except that the oscillations with unit-cell periodicity are not present.

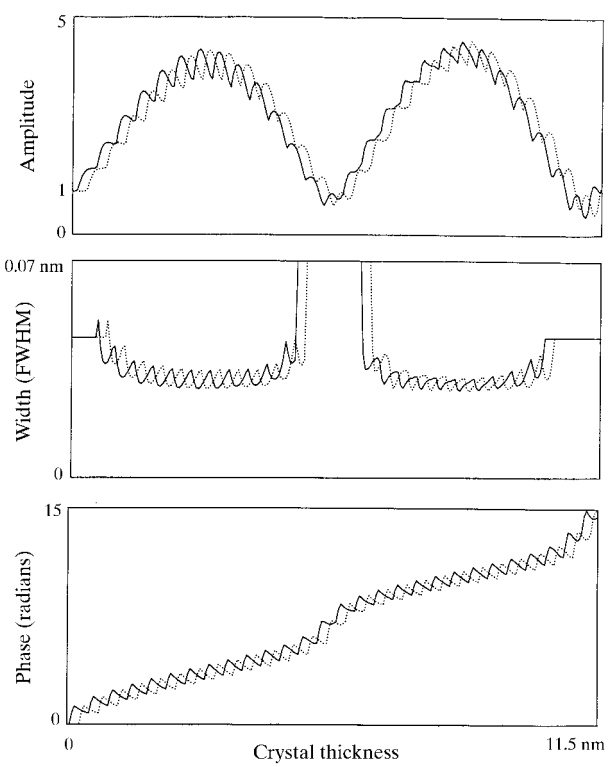

Fig. 1. The calculated amplitude, peak width and phase for 200 keV electrons channeled along the rows of atoms in a gold crystal in [001] orientation as functions of crystal thickness.

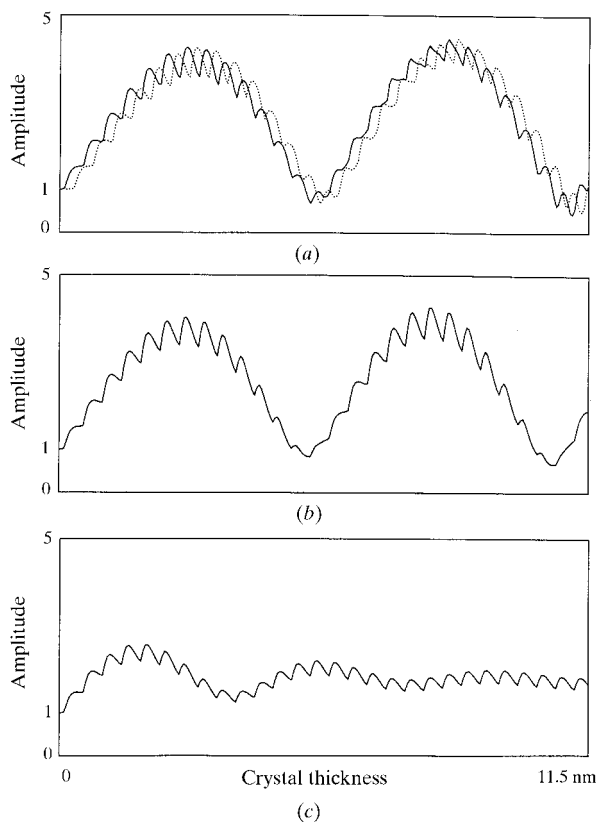

Fig. 2. Amplitude curves as in Fig. 1 but for incident beams that are (*a*) a plane wave, (*b*) a focused beam of diameter approximately 0.23 nm from a STEM instrument, and (*c*), a beam of diameter 0.082 nm from a hypothetical STEM instrument.

If, instead of a plane wave, the incident beam is the focused probe of a STEM instrument, the periodicity of the amplitude variation decreases but the minimum probe diameter is very little affected. This is illustrated in Fig. 2 in which the amplitude variation for a plane wave is repeated as Fig. 2(*a*) and is compared with that for a STEM probe for a STEM instrument with $C_s = 1$ mm, a defocus of -55 nm and an objective aperture size of 7.5 mrad (beam width 0.23 nm) in Fig. 2(*b*), and for an imaginary STEM instrument giving a crossover with 0.082 nm width in Fig. 2(*c*). For Fig. 2(*b*), the periodicity is reduced to 5.36 nm and for Fig. 2(*c*) it is greatly reduced to 3.74 nm. This result is consistent with that of Sanchez & Cowley (1998), who found a

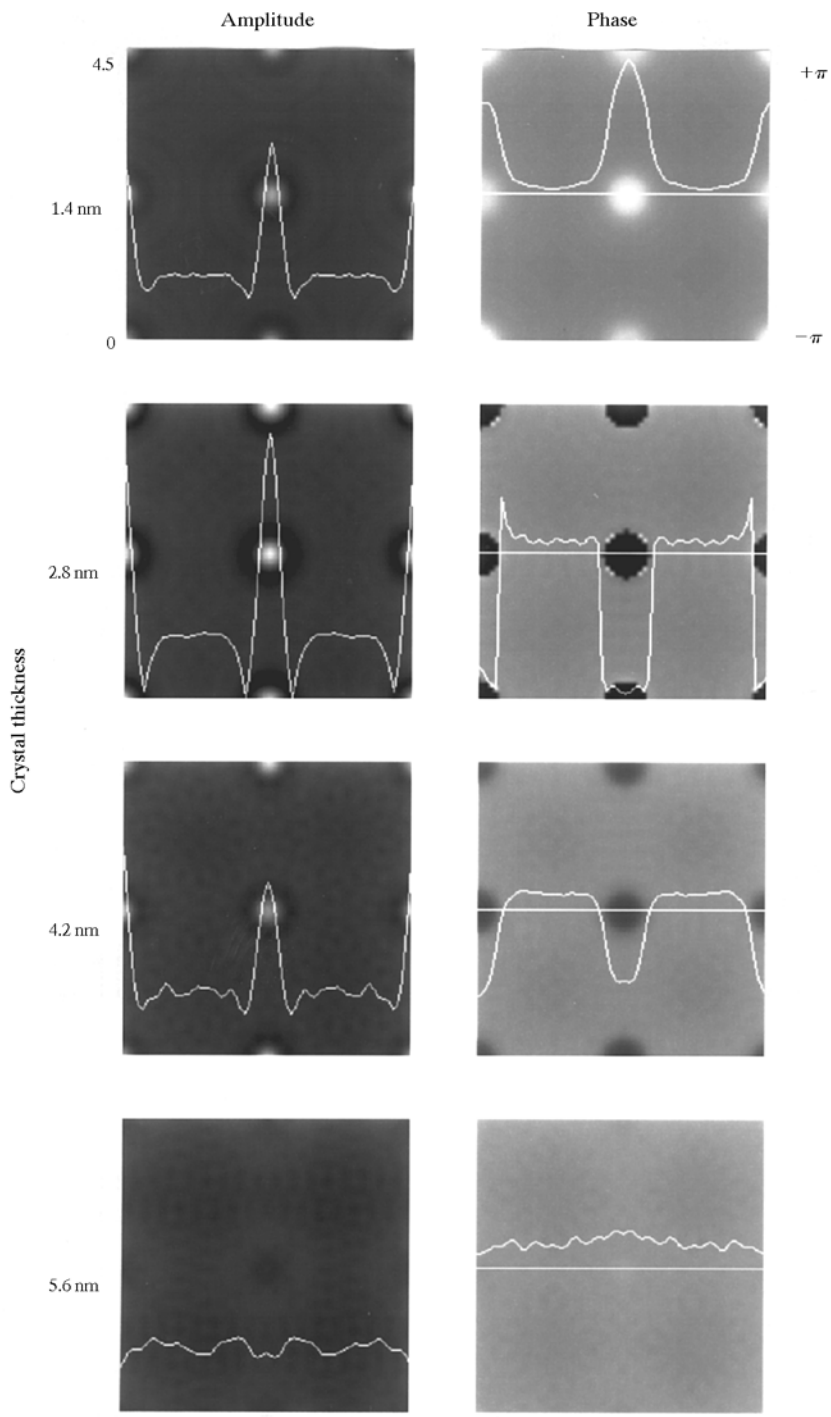

Fig. 3. The two-dimensional distributions of amplitude and phase across the projected unit cell for the case of Fig. 1 for various thicknesses, and the profiles of amplitude and phase along the line through the central atom position. The vertical bounds of the diagram correspond to phases of $-\pi$ and $+\pi$.

periodicity of about 3.6 nm for a beam, assumed to be Gaussian, of width 0.14 nm.

In the rest of the unit cell, away from the atom columns, the amplitude and phase show very little lateral variation. This is indicated by the parts of Fig. 3, which represent the two-dimensional distributions, and profiles across the central atom, for the amplitude and phase of the wave of Fig. 1 for various thicknesses of crystal. These figures confirm that it is a reasonable approximation to assume that the wave function at the exit face of a crystal can be described as a periodic array of real, sharp peaks plus a flat background of variable phase. This approximation was used by Cowley *et al.* (1998) as a convenient basis for deriving analytical expressions for the image contrast for the various modes of imaging employing atomic focusers. The phase of the background relative to that of the peak is seen to increase steadily to the value π for the crystal thickness of 2.8 nm, which gives the highest, sharpest peak.

3. Propagation beyond an atomic focuser crystal

Fig. 4 shows the variation of height and width of the peaks in the amplitude of the wavefunction along the direction of the rows of atoms of an Au[001] atomic focuser crystal as a function of the distance, z, beyond the exit face of the crystal for various crystal thicknesses, for 200 keV electrons with a plane wave incident. As may be expected, the curves show the periodicity of the Fourier image distance, $2a^2/\lambda$, of 33.2 nm. Also as expected, the same periodic variation, shifted by a distance of a^2/λ, in the z direction, occurs for the lines through the points with indices (0.25, 0.25) and (0.25, 0.75) *etc.* of the gold unit-cell projection.

In addition to the high sharp peaks at the Fourier-image distances, clearly visible in Fig. 4, there are intermediate peaks at submultiples of the Fourier-image distance. The presence of these peaks is readily explained on the basis of the simple theory of Fresnel diffraction in the small-angle approximation as follows.

The wave function in the space beyond the crystal may be written $\psi(\mathbf{r}, z)$, where $\mathbf{r}$ is a two–dimensional vector and one atom of the crystal exit face is taken as the origin. The two-dimensional Fourier transform of the wave at the exit face, $\psi(\mathbf{r}, 0)$, is written as $\Psi_0(\mathbf{u})$. For any distance z from the exit face, the wave function is given by the convolution of the exit wave function with the propagation function, which, in the small-angle approximation, is

$$p(\mathbf{r}, z) = (i/z\lambda)\exp[-i\pi|\mathbf{r}|^2/(z\lambda)], \qquad (1)$$

so that the wave function along the line $\mathbf{r} = 0$ becomes

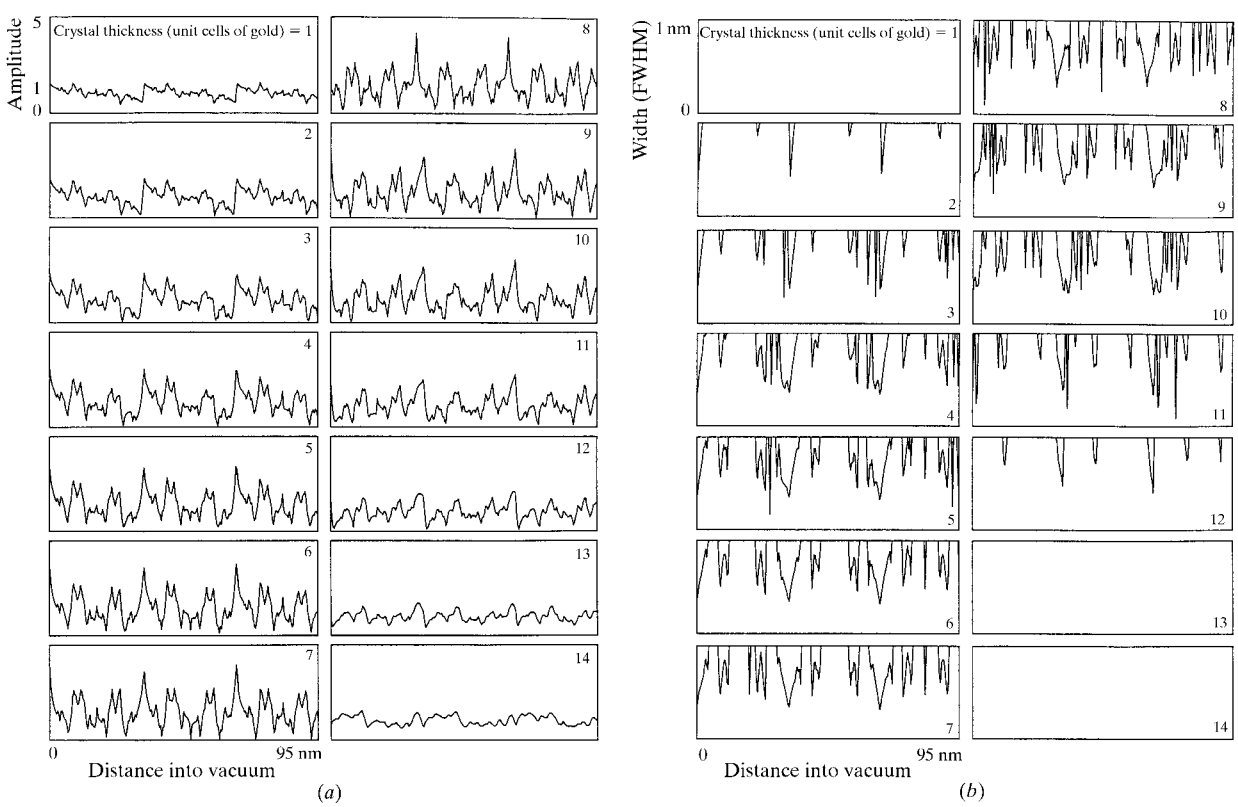

Fig. 4. (*a*) Peak amplitudes and (*b*) widths for the wave in vacuum along the lines through the atoms of Fig. 1 for various crystal thicknesses.

$$\psi(0, z) = (i/z\lambda) \int \psi(\mathbf{r}, 0) \exp[-i\pi|\mathbf{r}|^2/(z\lambda)]\, d\mathbf{r} \quad (2)$$

or, expressing $\psi(\mathbf{r}, 0)$ as the inverse Fourier transform of $\Psi_0(\mathbf{u})$,

$$\psi(0, z) = \int \Psi_0(\mathbf{u}) \exp[i\pi z\lambda|\mathbf{u}|^2]\, d\mathbf{u}. \quad (3)$$

Equations (2) and (3) may be thought of as expressing 'Fresnel transforms' and, to some extent, inverse operations may be written:

$$\psi(|\mathbf{r}|, 0) = (-i/z\lambda) \int \psi(0, z) \exp[i\pi|\mathbf{r}|^2/(z\lambda)]\, dz \quad (4)$$

$$\Psi_0(|\mathbf{u}|) = \int \psi(0, z) \exp[-i\pi z\lambda|\mathbf{u}|^2]\, dz, \quad (5)$$

so that the inverse operations give not the two-dimensional functions $\psi(\mathbf{r}, 0)$ and $\Psi_0(\mathbf{u})$ but these functions averaged circumferentially about constant distances from the origin.

If the sharp maxima in the wavefunction at the exit face of the crystal form a square lattice, as in the case of Au[001], (3) can be written

$$\psi(0, z) = \sum_{h,k} \Psi(h, k, 0) \exp[i\pi z\lambda(h^2 + k^2)/a^2]. \quad (6)$$

If we put $z = \eta 2a^2/\lambda$, so that η is the fraction of the Fourier-image distance, it is seen that, if all the $\Psi(h, k, 0)$ have the same sign and can be approximated by δ functions, as in the present case, maxima are to be expected in $\psi(0, z)$ for $\eta = n/(h^2 + k^2)$ for any integer n.

For the first-order Fourier image ($n = 1$), peaks are expected for $(h^2 + k^2) = 1, 2, 4, 5, 8, 9$. At first sight, it would seem anomalous that prominent peaks in the amplitude curve of Fig. 4 occur corresponding to $\eta = 1/3$. However, peaks at this position can be generated if larger values of n are included. For example, contributions to a peak at around 1/3 can come from values of $n/(h^2 + k^2)$ such as 3/9, 5/16, 6/18, 7/20 and so on.

The curves of Fig. 4 resolve the question of the degree to which the sharp crossovers created by atomic focusers extend into the vacuum beyond a crystal exit face. It is seen that for very small thicknesses the peak heights decrease and the peak widths increase, slowly over a distance of 1–2 nm from the exit face. For the optimum crystal thickness of about 3 nm (7 or 8 unit cells) or for odd-numbered multiples of this thickness, for which the peaks are highest and narrowest, the effective extension of the peak into the vacuum is reduced to 1 nm or less. For crystal thicknesses from 3 nm to about 6 nm, the extension of the peak into the vacuum decreases even further. It may be considered that the optimum sharp crossover is then 1 or 2 nm within the crystal. It is evident that, for those modes of imaging in STEM or TEM that rely on the use of the very narrow beam crossover within 1 or 2 nm of the crystal surface, it is essential to use crystals of thickness less than 3 nm (in the case of Au[001]) or of a thickness in one of the ranges of about 1 to 3 nm greater than the multiples of the periodicity of 5.56 nm.

For a crystal atomic focuser consisting of atoms of smaller atomic number, it is to be expected that the periodicity of the wavefunction along the column of atoms in the crystal will be greater. For example, for a crystal of copper in [001] orientation, the intensity along the lines of atoms is as shown in Fig. 5. The periodicity is increased to 11.5 nm. However, the decrease of the peak intensity outside the crystal appears to be much the same as for the gold crystal. The dashed lines of Fig. 5 indicate that the decay of the peak intensity into the vacuum for a crystal terminated at various thicknesses takes place over a distance of 1 or 2 nm, as for gold, and the decay becomes steeper as the thickness increases to the optimum thickness for maximum intensity, equal to about half the periodicity. The decay of peak height into the vacuum is again relatively slow for crystal thicknesses somewhat greater than the periodicity of 11.5 nm.

For those modes of TEM or STEM imaging with atomic focusers that rely on the use of the arrays of crossovers at the Fourier-image distances from the crystal, it is evident from the sharpness of the peaks in Fig. 4 that the depth of focus for imaging a thin specimen with optimum resolution is very small, of the order of 1 nm. The desirable distance of the specimen from the focuser is seen to vary by 1–2 nm as the thickness of the crystal is increased. The sharpness of the peaks in the curves, especially for the optimum thickness of about 3 nm, is such as to suggest that good image contrast may be achieved for the proposed application of atomic focusers for the preferential imaging of thin slices within a relatively thick specimen.

4. Imaging in the TEM Fourier-image mode

In the paper of Cowley *et al.* (1998), some initial simulations were reported for the case that a specimen is placed at a Fourier-image distance beyond a crystal, which serves as a periodic multiple atomic focuser, illuminated by a plane wave, and a TEM instrument is used to image the exit wave from the specimen, as

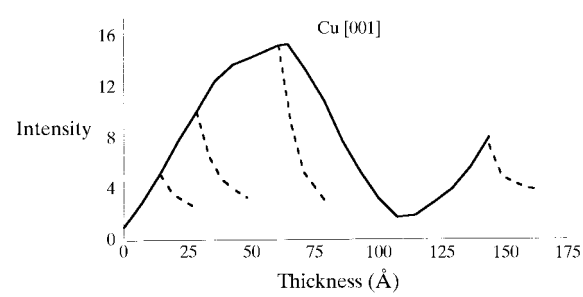

Fig. 5. The intensities of the peaks at the atom positions for a Cu[001] crystal. The solid line indicates the peak-height variation within the crystal. The dashed lines show the decay of the peak height in vacuum for a crystal terminated at various thicknesses.

suggested in Fig. 6. The Fourier image of the periodic array of fine crossovers formed at the exit face of the crystal may be scanned over the specimen by tilting the incident beam, and for each beam tilt a TEM image is recorded. From the resulting series of TEM images, it is then possible to derive an image of the specimen with a resolution corresponding to the width of the probes formed by each atomic focuser.

For a specimen consisting of two Au atoms, 0.05 nm apart, placed at the first Fourier image distance of 33.2 nm beyond a crystal multiple focuser, consisting of an Au[001] crystal of the optimum thickness of 2.8 nm, it was shown that it is possible to derive an image in which the two gold atoms are clearly resolved with the high contrast. In the simulation, the TEM instrument was assumed to have a resolution of 0.2 nm. Ultra-high-resolution imaging by this method may be applied to specimens of area limited only by the extent of the atomic focuser crystal and by the memory size of the computer used for correlation of the multiple TEM images.

More detailed simulations have now been made for the same geometry but with a more complicated specimen consisting of two Au atoms and a silicon atom placed at the vertices of a right-angle isosceles triangle with Au–Au and Au–Si separations of 0.05 nm. For convenience, this specimen is assumed to be periodic, with the array of three atoms repeated with the periodicity of the projected gold lattice. The TEM instrument is assumed to have $C_s = 1$ mm and an objective aperture of 40 mrad for 200 keV electrons, giving a nominal bright-field resolution of about 0.23 nm. Images have been calculated for various defocus values of the TEM instrument. Fig. 7(*a*) shows the projected potential distribution for this group of atoms. It is seen that, although the Au atoms are clearly separated in this projection, the Si atom appears as only a small bump on the side of an Au atom, not clearly separated. Fig. 7(*b*) shows a selection of images from a defocus series with differences of 1 nm between defocus values. Each image, 0.407×0.407 nm, is formed by correlating a set of 65×65 TEM images obtained with tilts of the incident

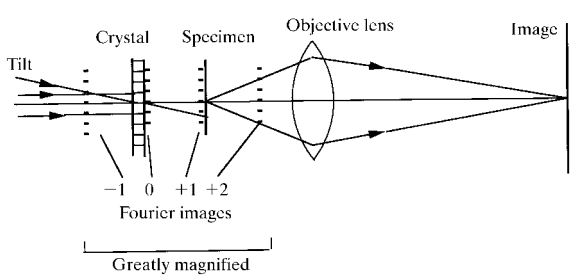

Fig. 6. Diagram of the arrangement in which a Fourier image of the amplitude distribution at the exit face of a thin crystal illuminates the specimen viewed with a conventional TEM instrument. The periodic array of fine crossovers is scanned over the specimen by tilting the incident beam.

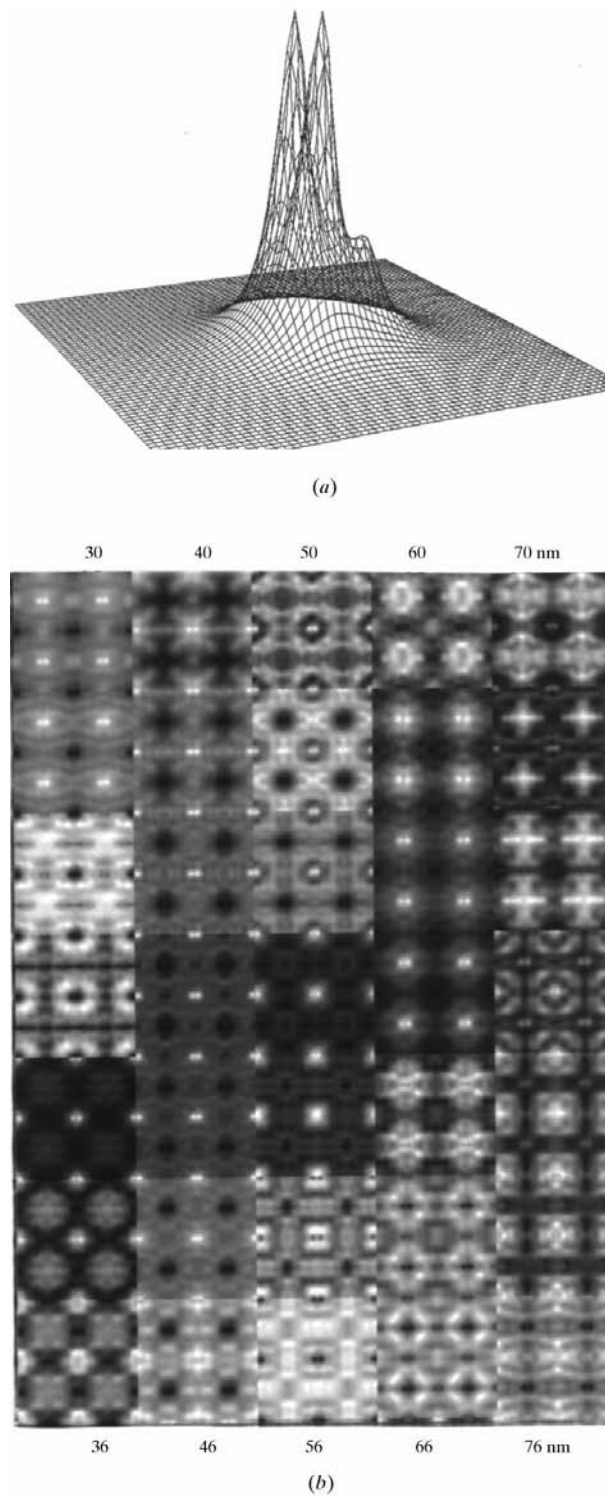

Fig. 7. (*a*) Projected potential for a specimen consisting of two Au atoms 0.05 nm apart plus an Si atom 0.05 nm from one of the Au atoms. (*b*) Ultra-high-resolution images of the specimen of (*a*) derived from the set of images formed by use of the scheme of Fig. 6 for various indicated values of the defocus (1 nm apart) of the TEM instrument.

beam in the range of ±6 mrad. Because, in this case, the specimen is assumed to be periodic, the images recur for the differences in defocus corresponding to the Fourier-image distance of 33.2 nm, and at the half-Fourier-image spacings, 16.6 nm, the images appear at the positions shifted by half an image periodicity in each direction.

Around −42 nm defocus, the image shows the two Au atoms as bright spots, clearly resolved, and the image of the Si atom is a weak extension of the peak of the right-hand Au atom, as might be expected from the projected potential distribution of Fig. 7(*a*). The half-Fourier images, with the images of the atoms displaced to surround the center positions of the periodic image cell, are seen at about 30 and 62 nm defocus.

5. Discussion

The simulations reported in the preceding section confirm that the TEM mode using a Fourier image of an atomic focuser crystal can produce ultra-high-resolution images of thin specimens showing only a slight smearing of the projected potential distributions. In the paper by Cowley *et al.* (1998), it was shown that equally good imaging may be obtained for the STEM mode, related by reciprocity to this TEM mode and represented by reversal of the direction of propagation of the electrons in Fig. 6.

For both of these modes, difficulties may arise in practice because of the need to hold the specimen at the Fourier image distance from the focuser crystal with an accuracy of about 1 nm. The possibility of adjusting the Fourier-image distance by variation of the incident electron accelerating voltage has been envisaged. For the TEM scheme, the requirement for recording and correlating many images to form the final ultra-high-resolution image implies relatively long exposure times and sensitivity to radiation damage and drift of the specimen. These factors should, however, be of no greater importance than for any other imaging process giving the same ultimate resolution. For the STEM scheme, the recording time for each image should be short but the specimen area of each image is very small. The total recording time is proportional to the total image area.

In the alternate TEM scheme, described in the paper of Sanchez & Cowley (1998) (and its STEM equivalent), similarly requiring no relative movement of the specimen and focuser crystal, the separation of the specimen and the focuser crystal is much smaller, about 1–2 nm. The difficulty of holding the specimen at a fixed distance from the exit face of the crystal focuser may possibly be overcome by the use of a very thin film of amorphous carbon or other light-atom material as a spacer. Present indications are that the images formed in these modes may suffer, however, from the presence of a strong bright spot with attendant ripples at the center of the image and a steeply falling intensity of the image with increasing radius. A more complete study of this mode is in progress.

When crystals containing lighter atoms than gold are used for the atomic focuser, the periodicities of the amplitude variation through the crystal are found to be greater. For barium ($Z = 56$), the periodicity is 8.0 nm. For copper ($Z = 29$), as seen in Fig. 5, the periodicity is 11.5 nm. These periodicities may also be affected, however, by the separations and densities of the atomic rows.

The lateral separations of the rows, in directions perpendicular to the beam direction, appear to have a relatively minor effect on the periodicities. Thus, calculations made for a hypothetical structure having only one atom per gold unit cell, for which the lateral separations of the Au-atom rows is 0.407 nm rather than 0.204 nm, show only a small difference in periodicity from the calculations for gold, but the successive maxima values tend to decrease with thickness as if some electrons are escaping from the channeled beams along the rows. There is a strong dependence on the separation of the atoms along the rows, in the beam direction. For gold in [111] orientation, with a separation of 0.702 nm along the rows in the beam direction, the periodicity is 9.5 nm, which implies that the periodicity corresponds to roughly the same number of Au atoms in the row as for the [001] direction. However, for the [110] orientation, with a separation of 0.288 nm, the periodicity is only 2.5 nm. This and the appearance of the curve of amplitude *versus* thickness, Fig. 8, suggest that the focusing effect per Au atom in the rows becomes stronger as the atoms are placed closer together. It is interesting to note that for these calculations, for which absorption effects are neglected, the maximum amplitude values increase and the minimum beam widths correspondingly decrease, with increasing thickness.

For those modes utilizing a perfect thin single crystal as a multiple atomic focuser, special considerations

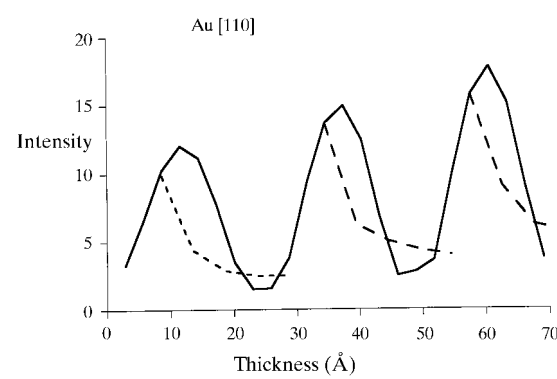

Fig. 8. Calculations of the heights of the peaks of intensity at the atom positions, as a function of thickness, for an Au [110] crystal. The solid line indicates the peak height within the crystal and the dashed lines suggest the decay of the peak height in vacuum for the crystal terminated at various thicknesses.

apply for the case that the specimen is also a thin perfect crystal. If the specimen crystal and the focuser crystal differ by only a small degree in periodicity or orientation, moiré patterns having a much larger periodicity may be formed. It was shown by Cowley & Moodie (1959) that, in favorable circumstances, with an objective aperture inserted to remove the contributions from the individual crystal periodicities, the intensity distribution of the moiré pattern may be given by the convolution of the transmission functions of the two crystals. If the periodicity of the moiré pattern is much greater than that of the focuser crystal, of known structure, it may be possible to deduce the structure of the specimen crystal with greatly improved resolution by deconvolution of the intensity distribution of the image formed in a conventional TEM.

This favorable situation was described by Cowley & Moodie (1959) for the case of very thin light-atom crystals for which the weak-phase-object approximation is reasonably well satisfied. It is clear from the results such as those of Figs. 1, 3 and 4 that equivalent, and even more favorable, situations arise for monoatomic focuser crystals having thicknesses that are close to being odd multiples of the optimum maximum-amplitude thicknesses when the separation of the specimen crystal from the focuser crystal is close to zero or a Fourier-image distance. Then the wavefunction incident on the specimen crystal is close to being a periodic set of δ-function peaks. If the specimen crystal is such that the weak-phase-object approximation applies, the intensity distribution of the image as seen in a conventional TEM gives the projected structure of the specimen crystal directly, greatly enlarged, with image detail corresponding to a resolution of the order of 0.05 nm or better. For more strongly scattering specimen crystals, the ultra-high-resolution image depends on dynamical diffraction effects to the same extent as for a conventional TEM image and can be interpreted in the same way, with the same limitations.

Such a simple interpretation of the moiré pattern intensities applies only for those cases where the differences of dimensions or orientation of the projected unit cells of the focuser and specimen crystals are sufficiently small. Relative to the projected unit cell of the specimen crystal, the peaks of the wavefunction from the focuser crystal should not come at positions more than about 0.02 nm apart in successive unit cells, so that a row of atoms in the specimen-crystal unit cell can be sampled at sufficiently small intervals. For more general situations, it is probably preferable to make use of the atomic focuser modes applicable for non-periodic objects.

References

Broeckx, J., Op de Beeck, M. & Van Dyck, D. (1995). *Ultramicroscopy*, **60**, 71–80.

Cowley, J. M., Dunin-Borkowski, R. E. & Hayward, M. C. (1998). *Ultramicroscopy*, **72**, 223–232.

Cowley, J. M. & Moodie, A. F. (1957). *Proc. Phys. Soc.* B**70**, 486–496.

Cowley, J. M. & Moodie, A. F. (1959). *Acta Cryst.* **12**, 423–428.

Cowley, J. M., Spence, J. C. H. & Smirnov, V. V. (1997). *Ultramicroscopy*, **68**, 135–148.

Fertig, J. & Rose, H. (1981). *Optik* (*Stuttgart*), **59**, 407–429.

Loane, R. F., Kirkland, E. J. & Silcox, J. (1988). *Acta Cryst.* A**44**, 912–927.

Marks, L. D. (1985). *Ultramicroscopy*, **18**, 33–38.

Rez, D., Rez, P. & Grant, I. (1994). *Acta Cryst.* A**50**, 481–497.

Sanchez, M. & Cowley, J. M. (1998). *Ultramicroscopy*, **72**, 213–222.

Saxton, W. O., Pitt, T. J. & Horner, M. (1979). *Ultramicroscopy*, **4**, 343–350.